

A Dual-Level Approach to Instanton Theory

Jan Meisner and Johannes Kästner*

Institute for Theoretical Chemistry, University of Stuttgart, Pfaffenwaldring 55, 70569 Stuttgart, Germany

E-mail: kaestner@theochem.uni-stuttgart.de

Abstract

Instanton theory is an established method to calculate rate constants of chemical reactions including atom tunneling. Technical and methodological improvements increased its applicability. Still, a large number of energy and gradient calculations is necessary to optimize the instanton tunneling path and 2nd derivatives of the potential energy along the tunneling path have to be evaluated, restricting the range of suitable electronic structure methods. To enhance the applicability of instanton theory, we present a dual-level approach in which instanton optimizations and Hessian calculations are performed using an efficient but approximate electronic structure method and the potential energy along the tunneling path is recalculated using a more accurate method. This procedure extends the applicability of instanton theory to high-level electronic structure methods for which analytic gradients may not be available, like local linear-scaling approaches. We demonstrate for the analytical Eckart barrier and three molecular systems how the dual-level instanton approach corrects for the largest part of the error caused by the inaccuracy of the efficient electronic structure method. This reduces the error of the calculated rate constants significantly.

Introduction

The accurate description of atom tunneling is crucial for the calculation of precise reaction

rate constants. An efficient yet accurate computational method to incorporate atom tunneling is semiclassical instanton theory.^{1–5} Instanton theory can be understood as a quantum mechanical analog to transition state theory (TST), thus, referred to as harmonic quantum transition state theory.^{6,7} The idea of instanton theory is to include nuclear quantum effects by statistical Feynman path integrals. Partition functions are approximated by the steepest descent approach, i.e. optimizing the most likely tunneling path, the so-called instanton, which is a 1st order saddle-point of the Euclidean action S_E , and taking fluctuations into account within the harmonic approximation.^{8–14} It is a successful compromise between accuracy and computational efficiency as it does not require a global potential energy surface, but can be used in combination with on-the-fly electronic structure calculations.^{15,16}

The applicability of instanton theory to the quantification of atom tunneling in molecular systems has been frequently demonstrated in the past decade.^{16–31} While traditionally instanton paths were often guessed or approximated using further assumptions,^{32–35} a modified Newton–Raphson (NR) instanton optimizer⁹ allows efficient instanton search for molecular systems with many degrees of freedom.^{9,22–31,36}

In practical applications, the instanton path \mathbf{y}_{inst} is discretized into P replicas or images. From these, the Euclidean action $S_E = S_0/2 +$

S_{pot} can be calculated with

$$S_0 = \frac{P}{\beta\hbar} \sum_{k=1}^P (\mathbf{y}_k - \mathbf{y}_{k-1})^2, \quad (1)$$

and

$$S_{\text{pot}} = \frac{\beta\hbar}{P} \sum_{k=1}^P V(\mathbf{y}_k). \quad (2)$$

Here, \mathbf{y}_k are the N mass-weighted coordinates of the k^{th} image, \hbar is the reduced Planck’s constant, $\beta = (k_{\text{B}}T)^{-1}$, T is the temperature, and k_{B} is Boltzmann’s constant. The reduced action S_0 is a measure of the path length and the distribution of the images along the path, while S_{pot} basically averages the potential along the instanton path. The potential $V(\mathbf{y}_k)$ at each image k is obtained from electronic structure calculations.

Instanton theory is, in its standard form, applicable only below a system-specific crossover temperature

$$T_c = \frac{\hbar\omega_{\text{b}}}{2\pi k_{\text{B}}} \quad (3)$$

which depends on the absolute value of the imaginary frequency of the transition state ω_{b} . Methods to extend it to above T_c are available,^{12–14,37} but will not be used here.

The instanton rate constant is obtained by

$$k_{\text{inst}} = \sqrt{\frac{S_0 P}{2\pi\beta\hbar^2}} \sqrt{\frac{\prod_{l=1}^{NP} \lambda_l^{\text{RS}}}{\prod_{l=1}^{NP} |\lambda_l^{\text{inst}}|}} \times \exp\left(-\frac{S_{\text{E}}(\text{inst}) - S_{\text{E}}(\text{RS})}{\hbar}\right). \quad (4)$$

Here, $S_{\text{E}}(\text{inst})$ refers to the Euclidean action of the instanton path, while $S_{\text{E}}(\text{RS})$ is the Euclidean action of the reactant state. In the latter, the optimal Feynman path is collapsed to the minimum on the potential energy surface, i.e. $S_0(\text{RS}) = 0$ and $S_{\text{E}}(\text{RS}) = \beta\hbar V(\mathbf{y}_{\text{RS}})$. The eigenvalues λ_l^{RS} and λ_l^{inst} refer to the second derivatives of S_{E} with respect to all coordinates of all images. To evaluate the latter, Hessians of $V(\mathbf{y}_k)$ have to be calculated for all images along the instanton path. One eigenvalue λ_l^{inst} is negative, seven are zero (six for linear molecules), all others are positive.¹⁵

The zero-eigenvalues are left out of the product, thus the prime in the product sign in equation (4). Together with the instanton optimization, the calculation of the Hessians is the most time-consuming step in computational applications of instanton theory. In one example described below, a sixteen-atomic molecular system (i.e. $N = 48$), the instanton is discretized into $P = 100$ images. This leads to a 2400-dimensional optimization problem (because the instanton, a closed Feynman path, covers the same line in configuration space twice, forward and backward). Even though the instanton optimization often requires just a few iterations,⁹ for every iteration $P/2 = 50$ energy and gradient evaluations are required. For the rate constant calculation, 50 Hessian calculations have to be carried out. These computations provide the rate constant for one value of the temperature. It is obvious that instanton calculations involve a significant computational effort.

In this paper, a dual-level approach to instanton theory is presented where for the time-consuming calculations a fast approximative method is applied to calculate $V(\mathbf{y})$. Subsequent energy calculations with a more accurate electronic structure method improve the quality of the calculated rate constant significantly.

Three different molecular systems were used to illustrate the performance of the dual-level instanton approach: the isomerization of HNC to HCN, an intramolecular [1,5] hydride shift, and the bimolecular hydrogen atom transfer reaction of $\text{NH}_2 + \text{H}_2 \rightarrow \text{NH}_3 + \text{H}$. For each system, reaction rate constants were calculated using the dual-level approach and are compared to the results of the conventional instanton theory at both the basic and accurate electronic potential.

Background and Computational Details

In computational chemistry, the evaluation of the electronic potential energy is often the most time-consuming step. One possible compromise to obtain reliable results within a reasonable time is a dual-level approach. An approximate,

but less demanding computational method is used for geometry optimizations and Hessian calculations in what will be referred to as the basic potential in the following. Subsequently, the potential energy is calculated using a more accurate, but more time consuming electronic structure method, which provides the refined potential. The fundamental assumption is that the basic potential is still able to reproduce the molecular geometries of the stationary points sufficiently accurate. Thermochemical results obtained in this way generally agree very well with results obtained with the refined potential. Also some calculations of rate constants using different tunneling corrections such as SCT and μ OMT utilized a dual-level approach successfully.^{38–40} Dual-level or even multi-level approaches have been used for the calculation of potential energy surfaces necessary for the computation of vibrational spectroscopy.⁴¹

Here, we show that the dual-level instanton approach leads to excellent results in terms of accuracy and computational effort. First the discretized instanton is optimized on the basic potential. Hessians of the potential energy are also calculated using the basic potential, providing λ_l^{RS} and λ_l^{inst} . Subsequently the energies at all images, $V(\mathbf{y}_k)$, as well as $V(\mathbf{y}_{\text{RS}})$ are calculated on the refined potential. Note, that no geometry optimizations at the refined potential are necessary, just energy calculations. From these, S_{pot} is obtained using the refined potential. This is assumed to correct the error caused by the inaccuracy of the basic potential. The working hypothesis is that the basic potential is able to reproduce the shape and image distribution of the instantons qualitatively well. The dual-level instanton rate constant reads

$$k_{\text{inst}}^{\text{Dual}} = \sqrt{\frac{S_0 P}{2\pi\beta\hbar^2}} \sqrt{\frac{\prod_{l=1}^{NP} \lambda_l^{\text{RS}}}{\prod_{l=1}^{NP} |\lambda_l^{\text{inst}}|}} \times \exp\left(\frac{-\frac{S_0(\text{inst})}{2} - \boxed{S_{\text{pot}}(\text{inst})} + \boxed{S_{\text{pot}}(\text{RS})}}{\hbar}\right) \quad (5)$$

where highlighting denotes the refined potential.

Hitherto, different studies combined approximate instanton methods with dual-level approaches^{33,34,42} or used basic-potential instantons as initial guess for the optimization of high-potential ones to obtain tunneling splittings.^{43,44} Only an instanton path fully optimized on the same potential energy surface as the one used for the Hessian calculations ensures the proper eigenvalue structure of λ_l^{inst} . Thus, in this work, instantons are optimized in all dimensions using the basic potential, *i.e.*, they are true 1st-order saddle points of the Euclidean action S_E . The refined potential is then used to correct S_{pot} .

For dual-level approaches in quantum chemistry, the nomenclature

Method_A/basis set_A // Method_B/basis set_B

is used. Here, *A* labels the level of theory and basis set of the refined potential and *B* refers to the basic potential. For simplicity, the basis set declaration is omitted in the shorthand notation

Method_A // Method_B

when possible.

In this work all geometry optimizations, including intrinsic reaction coordinates (IRCs) and instantons, as well as rate calculations were performed using the DL-FIND optimization library⁴⁵ interfaced to Chemshell.^{46,47} IRCs were optimized using a Hessian-predictor-corrector algorithm.⁴⁸ Instantons were optimized until the maximum component of the gradient is smaller than $1 \cdot 10^{-8}$ atomic units (scaled relative to the electron’s mass) using the adapted, quadratically convergent Newton–Raphson algorithm.^{9,10} CCSD(T)-F12a^{49,50} calculations were performed using molpro⁵¹ with default settings and the cc-pVDZ-F12 basis set throughout.⁵² All DFT calculations were performed with Turbomole version 7.0.1.⁵³ SCF energies were converged to an accuracy of 10^{-9} Hartree on an *m5* multi-grid.⁵⁴

For the Eckart barrier and reaction 1, $P = 200$ images were used, for reaction 2, $P = 100$ was used for all temperatures. For reaction 3, $P = 154$ images were used for the DFT instanton calculations. For the instantons calculated

on CCSD(T)-F12 level, 40 images were used down to 219 K, 78 images down to 131 K, and 154 and 306 images for 119 K and 109 K, respectively. Tests showed, that the rate constants were converged with respect to the number of images P within the comparisons done here.

This paper demonstrates the applicability of the dual-level instanton method. Here, the focus lies on the comparison of the dual-level instanton method with conventional instanton theory. As absolute values of the reaction rate constants are of less importance for this study, no comparison with literature values is done.

Results

The Eckart barrier

As a first example, we apply the dual-level scheme to the analytic one-dimensional Eckart⁵⁵ barrier in order to distinguish specific inaccuracies of the basic potential and their effects on the dual-level approach. We investigated several different scenarios of which we show one typical case and the one where we found the weakest performance of the dual-level approach in order to learn about the limits of the method.

The potential of the Eckart barrier is given by

$$V(x) = \frac{V_A y}{1+y} + \frac{V_B y}{(1+y)^2}, \quad (6)$$

$$y = \frac{V_A + V_B}{V_B - V_A} \exp(\alpha x). \quad (7)$$

Here V_A determines the exothermicity: while for large negative reaction coordinates x the potential becomes zero, it approaches V_A for large positive x . The maximum of $V(x)$ is at $x = 0$ and has the value

$$V_{\max} = \frac{(V_A + V_B)^2}{4V_B}. \quad (8)$$

For the refined potential we chose $V_A = -0.01$ Hartree (-26.3 kJ mol⁻¹) and $V_{\max} = 0.01$ Hartree. These two parameters are varied in the following to describe different basic potentials. The width α is adjusted in all cases such

that $T_c = 300$ K.

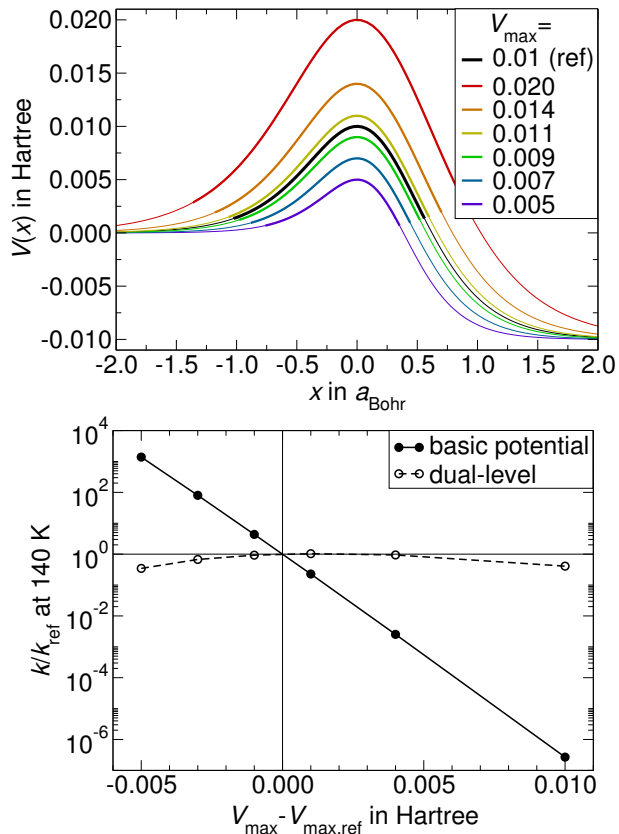


Figure 1: Effects of errors in the barrier height on the rate constants. Top: Barrier shapes for different values of V_{\max} , thicker lines indicate instantons at 140 K. Bottom: Deviation of the rate constant as function of the deviation of the barrier height.

The effect of an inaccurate description of the barrier height by the basic potential is illustrated in Fig. 1. If V_{\max} is varied from twice to half the reference value while keeping the reaction energy and T_c (and, thus, ω_b) constant, the resulting rate constant at 140 K increases by 3 or decreases by almost 7 orders of magnitude. The dual-level scheme (hollow symbols in the lower graph of Fig. 1) corrects for that very accurately, with remaining errors of less than a factor of 3. A wrong barrier height is the typical error of an approximate electronic structure method.

By contrast, the case where the barrier height is preserved, but the exothermicity is described wrongly is shown in Fig. 2. Since the rate constant primarily depends on the barrier height rather than the shape of the barrier at the prod-

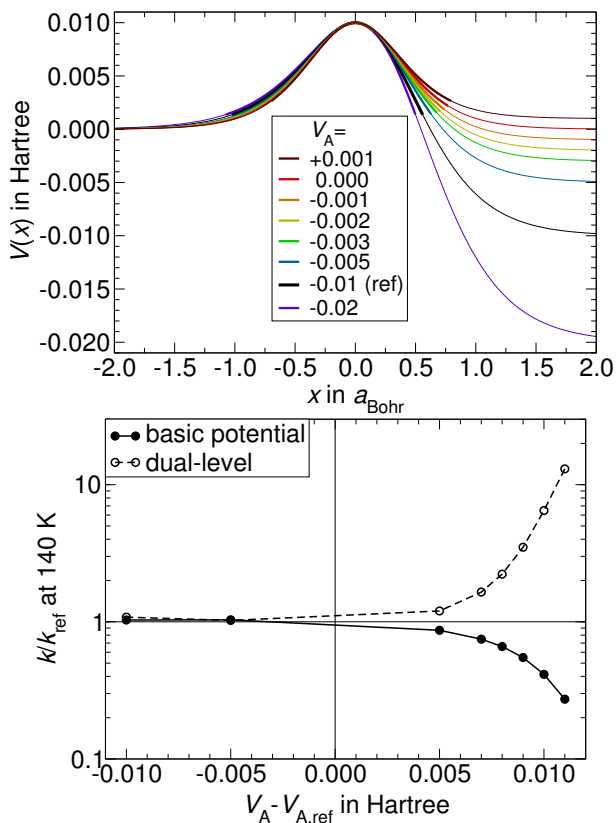


Figure 2: Effects of errors in the exothermicity ($-V_A$) on the rate constants. Top: Barrier shapes for different values of V_A , thicker lines indicate instantons at 140 K. Bottom: Deviation of the rate constant as function of the deviation of the exothermicity.

uct side, the changes caused in the rate constant are smaller. Especially if the basic potential predicts a too exothermic reaction, the influence on the rate constant is negligible. However, when the basic potential describes the reaction energy to be too positive, we find the extreme case where the dual-level approach fails, which can be seen from the lower graph of Fig. 2. Whenever the exothermicity is too low ($V_A - V_{A,\text{ref}} > 0$) the rate constant obtained by the dual-level scheme is less accurate than the non-corrected basic rate constants. The reason is that with a potential describing the reaction to be too endothermic, the distribution of the images is shifted more to the product side, which can not be corrected by the dual-level approach. The refined potential energy of these images on the product side is then erroneously low, which leads to an underestimation of S_E and an overestimation of the rate constant. The cause of this difference is the change in the potential energy in the region of the instanton, rather than in the product well. It should be noted that this is the most extreme case we found, and still the overall error is rather small.

Reaction 1: The Isomerization $\text{HNC} \rightarrow \text{HCN}$

The isomerization of HNC to HCN is a unimolecular prototype reaction with well-defined reactant state structure (HNC) and product state structure (HCN). Furthermore, the three-atomic system is small enough to carry out full conventional instanton calculations on the CCSD(T)-F12/cc-pVDZ-F12^{49,52,56} level, which was used as the refined potential. For the basic potential, B3LYP⁵⁷⁻⁶² was used in combination with the def2-SVP basis set.⁶³

The reaction energies ΔV of basic and refined potential deviate by 5.4 kJ mol^{-1} , see table 1. The potential activation barrier V_A of B3LYP is higher than the CCSD(T)-F12 value by only 6.6 kJ mol^{-1} . The crossover temperatures are also quite similar and deviate by just 15.9 K , that is $\approx 6 \%$.

The IRCs were optimized for both potentials, see Fig. 3. Additionally, CCSD(T)-F12 en-

Table 1: Potential energy barriers V_A , potential reaction energies ΔV and the respective values corrected by zero-point energy, E_A , and ΔE for reaction 1: $\text{HNC} \rightarrow \text{HCN}$. Energies in kJ mol^{-1} , T_c in K.

	Basic Potential	Refined potential	Dual-level
Method	B3LYP	CCSD(T)-F12	
Basis set	def2-SVP	cc-pVDZ-F12	
V_A	142.8	136.2	136.2
ΔV	-57.2	-62.6	-62.4
E_A	128.9	123.5	122.4
ΔE	-60.8	-65.5	-66.0
T_c	257.0	272.9	

ergy calculations were performed on the IRC optimized with B3LYP, shown as blue crosses in Fig. 3. That potential energy curve coincides with the potential energy along the IRC of CCSD(T)-F12, indicating that the IRC geometries are similar.

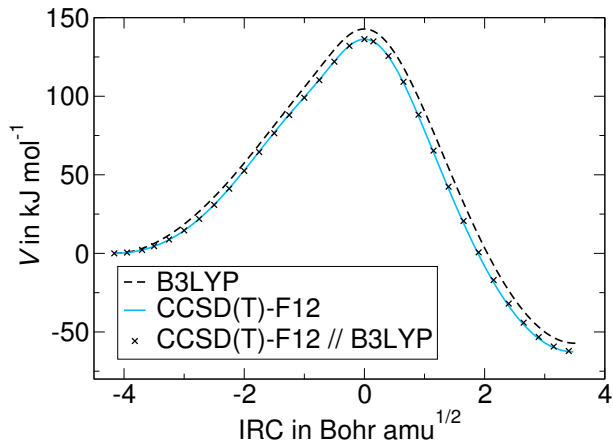


Figure 3: Potential energy along the IRCs of reaction 1.

Rate constants for reaction 1 are shown in Fig. 4 as Arrhenius plots, i.e. the logarithm of the rate constant is plotted against $1/T$. Rate constants were obtained by conventional instanton theory using both electronic potentials as well as the CCSD(T)-F12 // B3LYP dual-level method. For B3LYP and the dual-level method, reaction rate constants down to 60 K were calculated, for CCSD(T)-F12 down to only 100 K. Due to the higher activation barrier, the B3LYP reaction rate constants are lower than the CCSD(T)-F12 reaction rate constants by a factor of 51.4 at 200 K and by a factor of 961.1 at 100 K. The dual-level corrects

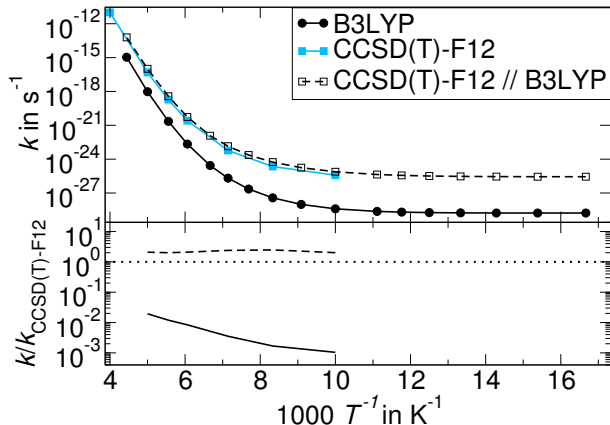


Figure 4: Top: Rate constants for reaction 1 with basic and refined potential as well as the dual-level method. Bottom: relative error of the rate constants with the basic potential and the dual-level method. The dotted line denotes $k = k_{\text{CCSD(T)-F12}}$, i.e. no error.

that error to factors between 2.0 and 2.5, see Fig. 4 and, thus, leads to excellent agreement with the results obtained with full calculations on the refined potential.

Using reaction 1 as an example we want to point out the savings in computational time: The optimization of one instanton and the subsequent rate calculation at CCSD(T)-F12a level require 19,744 and 30,449 seconds, respectively. On B3LYP level 626 and 1,305 seconds are required for the instanton optimization and rate calculation on the same computer infrastructure. The additional CCSD(T)-F12a energy calculations for the dual-level approach require 323 seconds. Derivatives on the CCSD(T)-F12a level were obtained from finite differences of energies, while DFT gradients were calculated an-

alytically. Thus, in this comparison, the dual-level approach saves a factor of > 20 in computational time.

Reaction 2: Intramolecular [1,5]-H-Shift

In sigmatropic rearrangements, tunneling was observed in many cases. Suprafacial [1,5] sigmatropic rearrangements were studied exhaustively, using derivatives of 1,3(*Z*)-pentadiene.^{64,65} Although it was initially unclear whether or not atom tunneling plays a crucial role in these reactions,^{66,67} various studies have confirmed its involvement.^{16,25,65,68–72} The [1,5] sigmatropic rearrangement of 1,3(*Z*)-hexadiene to 2(*E*),4(*Z*)-hexadiene, Fig. 5, is therefore an appropriate test system for the dual-level instanton method.

Two density functionals, the BP86 GGA functional^{57–60,73} and the BHLYP hybrid functional,^{57–61,74} both with the 6-31G* basis set,⁷⁵ were applied to obtain different electronic potentials.

This is a much more severe test for the dual-level, because the potential activation energy obtained by BHLYP is more than 56.8 kJ mol^{-1} higher than the one obtained by BP86, see table 2. This is attributed to the high amount (50%) of exact exchange in the BHLYP functional. CCSD(T)-F12a calculations on the BHLYP (BP86) geometries resulted in $V_A = 149.1 \text{ kJ mol}^{-1}$ ($148.9 \text{ kJ mol}^{-1}$) and $\Delta V = -11.3 \text{ kJ mol}^{-1}$ ($-11.4 \text{ kJ mol}^{-1}$) implying that the BHLYP/6-31G* method yields more reliable results than the BP86/6-31G* method. However, the two functionals are eminently suitable to demonstrate the applicability of the dual-level method in cases where the activation barrier of the two functionals differ significantly. In this context, it has to be mentioned that, although the activation barriers obtained by the

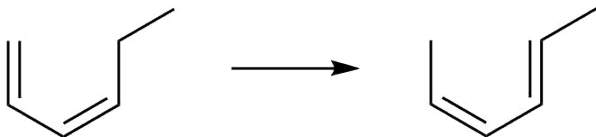


Figure 5: The [1,5] H shift in reaction 2.

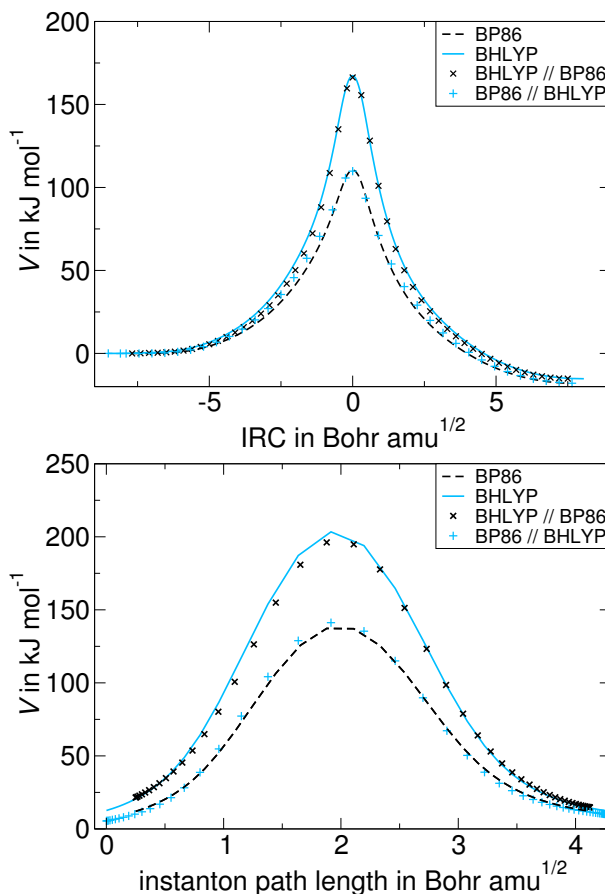


Figure 6: Potential energy along the IRCs of reaction 2 (top) and along instanton paths at 100K (bottom).

two functionals disagree, the reaction energies agree within 2.8 kJ mol^{-1} , see table 2. For both dual-level combinations, BHLYP // BP86 and BP86 // BHLYP, the potential energy along the IRC is restored quite well, as can be seen in Fig. 6. The bottom graph of Fig. 6 shows the potential energy along instantons at 100K. The energies are, again, well reproduced by the dual-level approach. The lengths of the instantons differ somewhat. Comparison of the upper and the lower graph additionally shows that the instanton path leads to regions in configuration space with significantly higher potential energy than the classical transition state ($203.4 \text{ vs } 167.4 \text{ kJ mol}^{-1}$ for BHLYP). This is caused by corner-cutting.

Instanton rate constants were calculated for a temperature range from 300 K to 100 K using the two density functionals, as well as both dual-level combinations, see Fig. 7. The lower activation barrier of the BP86 poten-

Table 2: Potential energy barriers V_A , potential reaction energies ΔV and the respective values corrected by zero-point energy, E_A and ΔE for reaction 2. Energies are in kJ mol^{-1} , crossover temperatures T_c in K.

Method	BP86	BHLYP	BP86 // BHLYP	BHLYP // BP86
Basis set	6-31G*	6-31G*		
V_A	110.6	167.4	109.8	166.3
ΔV	-18.0	-15.2	-18.1	-15.3
E_A	100.3	156.4	98.9	155.9
ΔE	-18.9	-16.4	-19.3	-16.3
T_c	308.8	394.7		

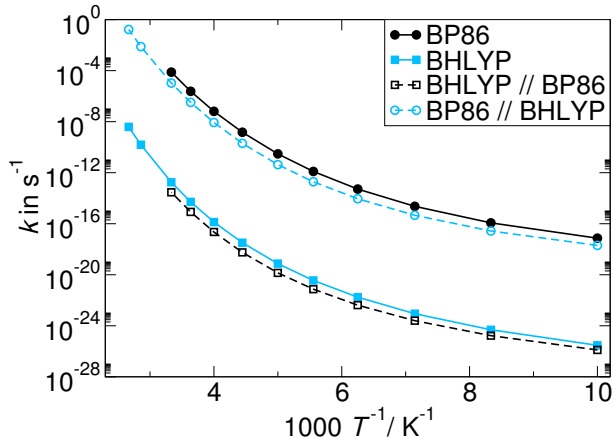


Figure 7: Rate constants for reaction 2.

tial compared to the BHLYP potential leads to much higher reaction rate constants, by more than eight orders of magnitude, throughout the whole temperature range. The curvature of all Arrhenius plots in Fig. 5, an indication of the importance of tunneling, is strikingly similar even though the crossover temperatures differ by more than 20 %. Despite the qualitative difference of both functionals, the results obtained with the dual-level instanton method reproduce the rate constants of the refined potential successfully in both cases. The values obtained by the dual-level approach agree with the full calculations of the respective refined potentials within one order of magnitude, see table 3. There, the average and maximum deviations (highest or lowest ratios) among the temperatures studied are shown. The small deviations are mainly due to error compensation. For BHLYP // BP86, the underestimation of S_0 is counterbalanced in the exponential term by an overestimation of S_{pot} . The remaining

error in the exponential dominates the total error, but is still counterbalanced by an opposite deviation in the pre-exponential factor.

Table 3: Ratios of rate constants for reaction 2.

	$\frac{k_{\text{BP86}}}{k_{\text{BHLYP}}}$	$\frac{k_{\text{BHLYP//BP86}}}{k_{\text{BHLYP}}}$	$\frac{k_{\text{BP86//BHLYP}}}{k_{\text{BP86}}}$
Max.	$4.75 \cdot 10^{+8}$	$1.63 \cdot 10^{-1}$	$1.34 \cdot 10^{-1}$
Avg.	$3.62 \cdot 10^{+8}$	$2.36 \cdot 10^{-1}$	$1.72 \cdot 10^{-1}$

Reaction 3: Bimolecular Reaction $\text{NH}_2 + \text{H}_2 \rightarrow \text{NH}_3 + \text{H}$

Finally, the dual-level approach is tested on the bimolecular hydrogen atom transfer reaction $\text{NH}_2 + \text{H}_2 \rightarrow \text{NH}_3 + \text{H}$. This five-atomic system with eleven electrons is small enough to be easily handled fully on the CCSD(T)-F12/cc-pVDZ-F12 level using conventional instanton theory as refined potential. BHLYP/def2-SVP was used as basic potential.

On CCSD(T)-F12 level, the electronic reaction energy is $-22.0 \text{ kJ mol}^{-1}$, while the vibrationally adiabatic reaction energy, i.e. the electronic energy plus zero-point vibrational energy, is -8.0 kJ mol^{-1} . During the reaction, an N-H bond is formed and a H-H bond is broken, leading to a large difference in zero-point vibrational energy between the reactants and products. The BP86 functional underestimates the exothermicity with and without zero-point energies. Thus, following from the results obtained for the Eckart barrier we would expect this case to be rather challenging for the dual-level approach. In the region of the

Table 4: Potential energy barriers V_A , potential reaction energies ΔV and the respective values corrected by zero-point energy, E_A and ΔE for reaction 3. Energies are in kJ mol^{-1} , crossover temperatures T_c in K.

	Basic Potential	Refined Potential	Dual-Level
Method	BHLYP	CCSD(T)-F12	
Basis set	def2-SVP	cc-pVDZ-F12	
V_A	35.5	41.5	40.7
ΔV	-15.1	-22.0	-23.2
E_A	44.2	48.8	49.3
ΔE	-0.8	-8.0	-9.0
T_c	355.9	355.8	

transition structure, the CCSD(T)-F12 energy calculations along the IRC calculated on the BP86 geometries resemble the energy along the CCSD(T)-F12-IRC well enough, however, see Fig. 8.

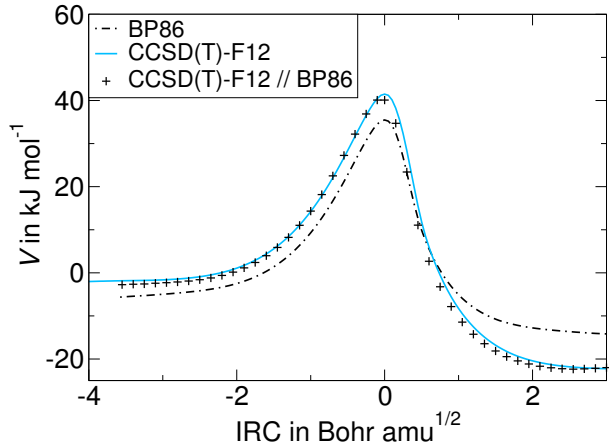


Figure 8: Potential energy along the IRCs of reaction 3 relative to the energy of the separated reactants.

The rate constants obtained with conventional instanton theory and the corresponding dual-level results are shown in Fig. 9. BP86 leads to higher reaction rate constants by a factor of 9–12 than the CCSD(T)-F12 reference throughout the temperature range of 300–110 K, caused by the lower activation barrier. The dual-level method successfully leads to reaction rate constants deviating only by a factor of less than 2 from the results obtained by conventional instanton theory using CCSD(T)-F12.

This finding is quite surprising as we would have expected the dual-level approach to fail

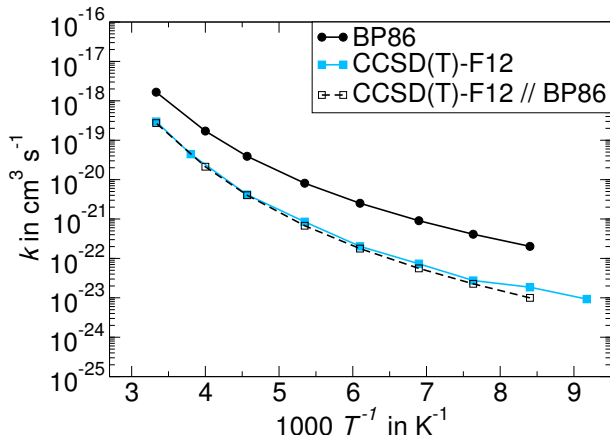


Figure 9: Rate constants for reaction 3.

due to the underestimated exothermicity. To understand that, let us recall the case of the Eckart barrier (Fig. 2). There, the potential energy is wrongly described on the right side of the potential energy barrier and affects the region of the instantons, leading to an incorrect shape and in particular image distribution. This caused the dual-level approach to be unsuitable. In the case of reaction 3, the final reaction energy is also described incorrectly. However, the instanton is restricted to the region in space where the energy is higher than the energy of the reactants, here to $s < +0.4$. There, the basic potential is sufficiently accurate and the shape and image distribution of the instantons is not affected. Thus, the dual-level approach is successful in this case.

Conclusion

We demonstrated the applicability of a dual-level approach to instanton theory by studying one analytic and three molecular systems. For the dual-level instanton calculations, all optimizations and Hessian calculations are carried out using a basic potential, which is computationally fast, but can be rather approximate. Additionally, energy calculations only are carried out for all images using a more accurate refined potential. We have shown that this approach corrects for the largest part of the errors in the rate constants by improving the value of S_{pot} in equation (5). The instanton geometry \mathbf{y}_{inst} , the distribution of the images, and therefore the value of S_0 (see equation (1)) are not changed and assumed to be described well enough by the basic potential.

The dual-level approach performs astonishingly well in the cases examined above. The calculated rate constants are similar to the rate constants obtained by conventional instanton calculations performed on the refined potential. For the isomerization reaction of HNC to HCN, the error with respect to full CCSD(T)-F12 results is reduced from factors of 50–1000 when using B3LYP to 2.0–2.5 for the CCSD(T)-F12 // B3LYP dual-level instanton approach.

The method works well even in the case when the activation barrier of the basic potential, one of the most crucial parameters when considering reaction rate constants, differs by more than 40% from the one obtained with the refined potential, like in reaction 2. There, the dual-level method reproduces the corresponding full instanton rate constants within one order of magnitude while without the dual-level scheme they differ by more than eight orders of magnitude.

In cases where the exothermicity of the reaction is underestimated, the dual-level method suffers from a wrong image distribution and hence can not correct for the errors in the potential energy, as seen from the Eckart barrier. However, this problem can easily be probed by performing reference calculations for the reaction energy. Furthermore it could be shown for the reaction of NH_2 and H_2 that the wrong description of the reaction energy is problematic

only if the region of the instantons is affected. Otherwise, the dual-level approach performs well. Obviously, there may be other causes of errors like a wrongly predicted topology or symmetry of the stationary points predicted by the basic potential which we could not identify in the cases we tested.

In summary, the dual-level approach can help improving the quality of instanton rate calculations when the systems are too big for the full treatment with highly accurate electronic structure methods. It is a legitimate improvement as long as the basic potential describes the chemical reaction qualitatively correct.

Acknowledgments

This work was financially supported by the German Research Foundation (DFG) within the Cluster of Excellence in Simulation Technology (EXC 310/2) at the University of Stuttgart. This work was financially supported by the European Union’s Horizon 2020 research and innovation programme (grant agreement No. 646717, TUNNELCHEM).

References

- (1) Langer, J. S. Theory of the condensation point. *Ann. Phys. (N.Y.)* **1967**, *41*, 108–157.
- (2) Miller, W. H. Semiclassical limit of quantum mechanical transition state theory for nonseparable systems. *J. Chem. Phys.* **1975**, *62*, 1899–1906.
- (3) Coleman, S. Fate of the false vacuum: Semiclassical theory. *Phys. Rev. D* **1977**, *15*, 2929–2936.
- (4) Callan Jr., C. G.; Coleman, S. Fate of the false vacuum. II. First quantum corrections. *Phys. Rev. D* **1977**, *16*, 1762–1768.
- (5) Gildener, E.; Patrascioiu, A. Pseudoparticle contributions to the energy spectrum of a one-dimensional system. *Phys. Rev. D* **1977**, *16*, 423–430.

- (6) Mills, G.; G. K. Schenter, D. M.; Jónsson, H. *Classical and Quantum Dynamics in Condensed Phase Simulations*; World Scientific, 1998; Chapter RAW Quantum Transition State Theory, p 405.
- (7) Andersson, S.; Nyman, G.; Arnaldsson, A.; Manthe, U.; Jónsson, H. Comparison of Quantum Dynamics and Quantum Transition State Theory Estimates of the $\text{H} + \text{CH}_4$ Reaction Rate. *J. Phys. Chem. A* **2009**, *113*, 4468–4478.
- (8) Richardson, J. O.; Althorpe, S. C. Ring-polymer molecular dynamics rate-theory in the deep-tunneling regime: Connection with semiclassical instanton theory. *J. Chem. Phys.* **2009**, *131*, 214106.
- (9) Rommel, J. B.; Goumans, T. P. M.; Kästner, J. Locating instantons in many degrees of freedom. *J. Chem. Theory Comput.* **2011**, *7*, 690–698.
- (10) Rommel, J. B.; Kästner, J. Adaptive integration grids in instanton theory improve the numerical accuracy at low temperature. *J. Chem. Phys.* **2011**, *134*, 184107.
- (11) Richardson, J. O. Derivation of instanton rate theory from first principles. *J. Chem. Phys.* **2016**, *144*, 114106.
- (12) Richardson, J. O. Microcanonical and thermal instanton rate theory for chemical reactions at all temperatures. *Faraday Discuss.* **2016**, *195*, 49–67.
- (13) McConnell, S. R.; Löhle, A.; Kästner, J. Rate constants from instanton theory via a microcanonical approach. *J. Chem. Phys.* **2017**, *146*, 074105.
- (14) McConnell, S.; Kästner, J. Instanton rate constant calculations close to and above the crossover temperature. *J. Comput. Chem.* **2017**, *38*, 2570–2580.
- (15) Kästner, J. Theory and Simulation of Atom Tunneling in Chemical Reactions. *WIREs Comput. Mol. Sci.* **2014**, *4*, 158–168.
- (16) Meisner, J.; Kästner, J. Atom-Tunneling in Chemistry. *Angew. Chem. Int. Ed.* **2016**, *55*, 5400–5413.
- (17) Mills, G.; Jónsson, H. Quantum and thermal effects in H_2 dissociative adsorption: Evaluation of free energy barriers in multi-dimensional quantum systems. *Phys. Rev. Lett.* **1994**, *72*, 1124–1127.
- (18) Mills, G.; Schenter, G. K.; Makarov, D. E.; Jónsson, H. Generalized path integral based quantum transition state theory. *Chem. Phys. Lett.* **1997**, *278*, 91–96.
- (19) Goumans, T. P. M.; Kästner, J. Hydrogen-Atom Tunneling Could Contribute to H_2 Formation in Space. *Angew. Chem. Int. Ed.* **2010**, *49*, 7350–7352.
- (20) Jónsson, H. Simulation of surface processes. *Proc. Nat. Acad. Sci. U.S.A.* **2010**, *108*, 944–949.
- (21) Goumans, T. P. M. Hydrogen chemisorption on polycyclic aromatic hydrocarbons via tunnelling. *Mon. Notices Royal Astron. Soc.* **2011**, *415*, 3129–3134.
- (22) Goumans, T. P. M.; Kästner, J. Deuterium Enrichment of Interstellar Methanol Explained by Atom Tunneling. *J. Phys. Chem. A* **2011**, *115*, 10767.
- (23) Meisner, J.; Rommel, J. B.; Kästner, J. Kinetic isotope effects calculated with the instanton method. *J. Comput. Chem.* **2011**, *32*, 3456–3463.
- (24) Álvarez-Barcia, S.; Flores, J. R.; Kästner, J. Tunneling Above the Crossover Temperature. *J. Phys. Chem. A* **2014**, *118*, 78–82.
- (25) Kryvohuz, M. Calculation of Kinetic Isotope Effects for Intramolecular Hydrogen Shift Reactions Using Semiclassical Instanton Approach. *J. Phys. Chem. A* **2014**, *118*, 535–544.
- (26) Richardson, J. O.; Pérez, C.; Lobsiger, S.; Reid, A. A.; Temelso, B.; Shields, G. C.;

- Kisiel, Z.; Wales, D. J.; Pate, B. H.; Althorpe, S. C. Concerted hydrogen-bond breaking by quantum tunneling in the water hexamer prism. *Science* **2016**, *351*, 1310–1313.
- (27) Beyer, A. N.; Richardson, J. O.; Knowles, P. J.; Rommel, J.; Althorpe, S. C. Quantum Tunneling Rates of Gas-Phase Reactions from On-the-Fly Instanton Calculations. *J. Phys. Chem. Lett.* **2016**, *7*, 4374–4379.
- (28) Song, L.; Kästner, J. Formation of the prebiotic molecule NH_2CHO on astronomical amorphous solid water surfaces: accurate tunneling rate calculations. *Phys. Chem. Chem. Phys.* **2016**, *18*, 29278–29285.
- (29) Lamberts, T.; Fedoseev, G.; Kästner, J.; Ioppolo, S.; Linnartz, H. Importance of tunneling in H-abstraction reactions by OH radicals - The case of $\text{CH}_4 + \text{OH}$ studied through isotope-substituted analogs. *Astron. Astrophys.* **2017**, *599*, A132.
- (30) Lamberts, T.; Kästner, J. Influence of Surface and Bulk Water Ice on the Reactivity of a Water-forming Reaction. *Astrophys. J.* **2017**, *846*, 43.
- (31) Song, L.; Kästner, J. Tunneling rate constants for $\text{H}_2\text{CO} + \text{H}$ on amorphous solid water surfaces. *Astrophys. J.* **2017**, *850*, 118.
- (32) Siebrand, W.; Smedarchina, Z.; Zgierski, M. Z.; Fernandez-RAMOS, A. Proton tunnelling in polyatomic molecules: A direct-dynamics instanton approach. *Int. Rev. Phys. Chem.* **1999**, *18*, 5–41.
- (33) Smedarchina, Z.; Fernandez-Ramos, A.; Rios, M. A. A comparison of two methods for direct tunneling dynamics: Hydrogen exchange in the glycolate anion as a test case. *J. Chem. Phys.* **1997**, *106*, 3956–3964.
- (34) Tautermann, C. S.; Voegelé, A. F.; Loerting, T.; Liedl, K. R. The optimal tunneling path for the proton transfer in malonaldehyde. *J. Chem. Phys.* **2002**, *117*, 1962–1966.
- (35) Tautermann, C. S.; Voegelé, A. F.; Loerting, T.; Liedl, K. R. An accurate semiclassical method to predict ground-state tunneling splittings. *J. Chem. Phys.* **2002**, *117*, 1967–1974.
- (36) Rommel, J. B.; Liu, Y.; Werner, H.-J.; Kästner, J. Role of Tunneling in the Enzyme Glutamate Mutase. *J. Phys. Chem. B* **2012**, *116*, 13682–13689.
- (37) Zhang, Y.; Rommel, J. B.; Cvitaš, M. T.; Althorpe, S. C. Shallow-tunnelling correction factor for use with Wigner-Eyring transition-state theory. *Phys. Chem. Chem. Phys.* **2014**, *16*, 24292–24300.
- (38) Corchado, J. C.; Espinosa-García, J.; Roberto-Neto, O.; Chuang, Y.-Y.; Truhlar, D. G. Dual-Level Direct Dynamics Calculations of the Reaction Rates for a Jahn-Teller Reaction: Hydrogen Abstraction from CH_4 or CD_4 by $\text{O}(^3\text{P})$. *J. Phys. Chem. A* **1998**, *102*, 4899–4910.
- (39) Sekušak, S.; Cory, M. G.; Bartlett, R. J.; Sabljčić, A. Dual-Level Direct Dynamics of the Hydroxyl Radical Reaction with Ethane and Haloethanes: Toward a General Reaction Parameter Method. *J. Phys. Chem. A* **1999**, *103*, 11394–11405.
- (40) Huang, C.-H.; Tsai, L.-C.; Hu, W.-P. Dual-Level Direct Dynamics Study on the Diels-Alder Reaction of Ethylene and 1,3-Butadiene. *J. Phys. Chem. A* **2001**, *105*, 9945–9953.
- (41) Pflüger, K.; Paulus, M.; Jagiella, S.; Burkert, T.; Rauhut, G. Multi-level vibrational SCF calculations and FTIR measurements on furazan. *Theor. Chem. Acc.* **2005**, *114*, 327–332.
- (42) Smedarchina, Z.; Siebrand, W.; Fernández-Ramos, A. The rainbow instanton method: A new approach to

- tunneling splitting in polyatomics. *J. Chem. Phys.* **2012**, *137*, 224105.
- (43) Mil'nikov, G. V.; Yagi, K.; Taketsugu, T.; Nakamura, H.; Hirao, K. Tunneling splitting in polyatomic molecules: Application to malonaldehyde. *J. Chem. Phys.* **2003**, *119*, 10–13.
- (44) Mil'nikov, G. V.; Yagi, K.; Taketsugu, T.; Nakamura, H.; Hirao, K. Simple and accurate method to evaluate tunneling splitting in polyatomic molecules. *J. Chem. Phys.* **2004**, *120*, 5036–5045.
- (45) Kästner, J.; Carr, J. M.; Keal, T. W.; Thiel, W.; Wander, A.; Sherwood, P. DL-FIND: an Open-Source Geometry Optimizer for Atomistic Simulations. *J. Phys. Chem. A* **2009**, *113*, 11856.
- (46) Sherwood, P.; de Vries, A. H.; Guest, M. F.; Schreckenbach, G.; Catlow, C. R. A.; French, S. A.; Sokol, A. A.; Bromley, S. T.; Thiel, W.; Turner, A. J. et al. QUASI: A general purpose implementation of the QM/MM approach and its application to problems in catalysis. *J. Mol. Struct. (THEOCHEM)* **2003**, *632*, 1–28.
- (47) Metz, S.; Kästner, J.; Sokol, A. A.; Keal, T. W.; Sherwood, P. ChemShell—a modular software package for QM/MM simulations. *WIREs Comput. Mol. Sci.* **2014**, *4*, 101–110.
- (48) Meisner, J.; Markmeyer, M. N.; Bohner, M. U.; Kästner, J. Comparison of classical reaction paths and tunneling paths studied with the semiclassical instanton theory. *Phys. Chem. Chem. Phys.* **2017**, *19*, 23085–23094.
- (49) Adler, T. B.; Knizia, G.; Werner, H.-J. A simple and efficient CCSD(T)-F12 approximation. *J. Chem. Phys.* **2007**, *127*, 221106.
- (50) Adler, T. B.; Werner, H.-J. Local explicitly correlated coupled-cluster methods: Efficient removal of the basis set incompleteness and domain errors. *J. Chem. Phys.* **2009**, *130*, 241101.
- (51) Werner, H.-J.; Knowles, P. J.; Knizia, G.; Manby, F. R.; Schütz, M. Molpro: a general-purpose quantum chemistry program package. *WIREs Comput. Mol. Sci.* **2012**, *2*, 242–253.
- (52) Peterson, K. A.; Adler, T. B.; Werner, H.-J. Systematically convergent basis sets for explicitly correlated wavefunctions: The atoms H, He, B–Ne, and Al–Ar. *J. Chem. Phys.* **2008**, *128*, 084102.
- (53) TURBOMOLE V, a development of University of Karlsruhe and Forschungszentrum Karlsruhe GmbH, 1989-2007, TURBOMOLE GmbH, since 2007; available from <http://www.turbomole.com>.
- (54) Eichkorn, K.; Weigend, F.; Treutler, O.; Ahlrichs, R. Auxiliary basis sets for main row atoms and transition metals and their use to approximate Coulomb potentials. *Theor. Chem. Acc.* **1997**, *97*, 119–124.
- (55) Eckart, C. The Penetration of a Potential Barrier by Electrons. *Phys. Rev.* **1930**, *35*, 1303–1309.
- (56) Knizia, G.; Adler, T. B.; Werner, H.-J. Simplified CCSD(T)-F12 methods: Theory and benchmarks. *J. Chem. Phys.* **2009**, *130*, 054104.
- (57) Dirac, P. Quantum Mechanics of Many-Electron Systems. *Proc. Royal Soc. (London) A* **1929**, *123*, 714–733.
- (58) Slater, J. A simplification of the Hartree-Fock method. *Phys. Rev.* **1951**, *81*, 385–390.
- (59) Vosko, S. H.; Wilk, L.; Nusair, M. Accurate spin-dependent electron liquid correlation energies for local spin density calculations: a critical analysis. *Can. J. Phys.* **1980**, *58*, 1200–1211.

- (60) Becke, A. Density-functional exchange-energy approximation with correct asymptotic behavior. *Phys. Rev. A* **1988**, *38*, 3098–3100.
- (61) Lee, C.; Yang, W.; Parr, R. G. Development of the Colle-Salvetti correlation-energy formula into a functional of the electron density. *Phys. Rev. B* **1988**, *37*, 785–789.
- (62) Becke, A. D. Density-functional thermochemistry. III. The role of exact exchange. *J. Chem. Phys.* **1993**, *98*, 5648.
- (63) Weigend, F.; Ahlrichs, R. Balanced basis sets of split valence, triple zeta valence and quadruple zeta valence quality for H to Rn: Design and assessment of accuracy. *Phys. Chem. Chem. Phys.* **2005**, *7*, 3297–3305.
- (64) Dormans, G. J. M.; Buck, H. M. The mechanism of the thermal [1,5]-H shift in cis-1,3-pentadiene. Kinetic isotope effect and vibrationally assisted tunneling. *J. Am. Chem. Soc.* **1986**, *108*, 3253–3258.
- (65) Liu, Y. P.; Lynch, G. C.; Truong, T. N.; Lu, D.; Truhlar, D. G.; Garrett, B. C. Molecular modeling of the kinetic isotope effect for the [1,5]-sigmatropic rearrangement of cis-1,3-pentadiene. *J. Am. Chem. Soc.* **1993**, *115*, 2408–2415.
- (66) Doering, W. v. E.; Zhao, X. Effect on Kinetics by Deuterium in the 1,5-Hydrogen Shift of a Cisoid-Locked 1,3(Z)-Pentadiene, 2-Methyl-10-methylenebicyclo[4.4.0]dec-1-ene: Evidence for Tunneling? *J. Am. Chem. Soc.* **2006**, *128*, 9080–9085.
- (67) Doering, W. v. E.; Keliher, E. J. Effect of Deuterium on the Kinetics of 1,5-Hydrogen Shifts: 5-Dideuteriomethylene-2,4,6,7,9-pentamethyl-11,11a-dihydro-12H-naphthacene. *J. Am. Chem. Soc.* **2007**, *129*, 2488–2495.
- (68) Vaníček, J.; Miller, W. H. Efficient estimators for quantum instanton evaluation of the kinetic isotope effects: Application to the intramolecular hydrogen transfer in pentadiene. *J. Chem. Phys.* **2007**, *127*, 114309.
- (69) Shelton, G. R.; Hrovat, D. A.; Borden, W. T. Tunneling in the 1,5-Hydrogen Shift Reactions of 1,3-Cyclopentadiene and 5-Methyl-1,3-Cyclopentadiene. *J. Am. Chem. Soc.* **2007**, *129*, 164–168.
- (70) Peles, D. N.; Thoburn, J. D. Multidimensional Tunneling in the [1,5] Shift in (Z)-1,3-Pentadiene: How Useful Are Swain–Schaad Exponents at Detecting Tunneling. *J. Org. Chem.* **2008**, *73*, 3135–3144.
- (71) Zimmermann, T.; Vaníček, J. Three applications of path integrals: equilibrium and kinetic isotope effects, and the temperature dependence of the rate constant of the [1,5] sigmatropic hydrogen shift in (Z)-1,3-pentadiene. *J. Mol. Model.* **2010**, *16*, 1779–1787.
- (72) Kryvohuz, M.; Marcus, R. A. Semiclassical evaluation of kinetic isotope effects in 13-atomic system. *J. Chem. Phys.* **2012**, *137*, 134107.
- (73) Perdew, J. P. Density-functional approximation for the correlation energy of the inhomogeneous electron gas. *Phys. Rev. B* **1986**, *33*, 8822–8824.
- (74) Becke, A. D. A new mixing of Hartree-Fock and local density-functional theories. *J. Chem. Phys.* **1993**, *98*, 1372–1377.
- (75) Hariharan, P. C.; Pople, J. A. The influence of polarization functions on molecular orbital hydrogenation energies. *Theor. Chim. Acta* **1973**, *28*, 213–222.

TOC Graphic

